Macromolecules
ARTICLE

Macromolecules **2009**, *42*, 7903–7912 **7903**
DOI: 10.1021/ma901329n

Insoluble Patterns of Cross-Linkable Conjugated Polymers from Blend Demixing in Spin Cast Films

Ana Charas,*,† Quirina Ferreira,† Joana Farinhas,†,‡ Manuel Matos,†,‡ Luís Alcácer,†,§ and Jorge Morgado†,§

†*Instituto de Telecomunicações, Instituto Superior Técnico, Avenida Rovisco Pais 1, 1049-001, Lisbon, Portugal,* ‡*Dep. Eng. Química, Instituto Superior de Engenharia de Lisboa, Lisbon, Portugal, and* §*Dep. Eng. Química e Biológica, Instituto Superior Técnico, Avenida Rovisco Pais 1, 1049-001, Lisbon, Portugal*

Received June 20, 2009; Revised Manuscript Received September 6, 2009

ABSTRACT: Insoluble patterns of cross-linkable conjugated polymers, CPs, are obtained from spin coating their blends with polystyrene, PS, following an approach first demonstrated for poly [2-methoxy-5-(2′-ethyl)hexyloxy-2,4-phenylenevinylene] (MEH-PPV) by Castro et al. (*Chem. Mater.* **2006**, *18*, 5504). Taking advantage of the CP and PS tendency to phase separate, we make use of CP functionality to be cross-linked, so PS can be removed, leaving behind a solvent-resistant pattern. Columnar, spike, and porous structures can be obtained. Furthermore, we show that these patterns morphologies and dimensions can be controlled by adjusting the experimental conditions and the PS molecular weight. We present strategies to tune cross-linkable CP's films morphologies aiming for applications in organic solar cells and light-emitting devices.

1. Introduction

Conjugated polymers, CPs, are being explored in a wide range of functions for low cost organic electronics. They combine several functional properties, such as electronic (semiconducting and conducting) and optical (luminescence and nonlinear optics). In addition, they can be flexible and processed from solution. One of the most relevant characteristics is the possibility of tuning their properties by molecular design. This relates not only to single-molecule properties but also to their supramolecular organization and morphology. In the broad new technological area of organic electronics and optoelectronics, CPs are being used as charge transport layers, light emitters, sensing elements, or photovoltaic active layers. It has been extensively documented that the polymer film morphology can deeply affect electronic processes and device characteristics. Furthermore, to fabricate integrated and/or pixelated systems, their patterning at small dimensions is needed. As a result, there has been an increasing expansion of methods to pattern CPs and their description has been the subject of recent reviews.[1,2] In this context, several nonreactive techniques, such as screen printing,[3] inkjet printing,[4] and soft lithography[5]have been adjusted to fabricate patterns of semiconducting polymers at micrometer and submicrometer dimensions. Other strategies to selectively deposit CPs rely on the reactivity of monomers or surfaces: surface chemistry has been employed to generate substrate templates where polymer patterns with micro- to submicrometric dimensions are produced through self-organization of polymer blends[6,7]or through electropolymerization of reactive monomers if the substrate is an electrode patterned with a self-assembled monolayer.[8−14] Patterned films can also be fabricated by spin-casting, only making use of the phase separation that occurs in polymer blends deposited on a given homogeneous surface, due to their low entropy of mixing. The phase separation degree is controlled not only by the thermodynamics but also by the kinetics, as pseudoequilibrium states can be frozen. This can be accomplished either by thermal quenching or solvent quenching using poor solvents. Phase separation occurring during fast solvent removal (solvent quenching) in spin-cast films has been widely investigated for insulating polymer blends, leading to nonequilibrium film morphologies, which are strongly affected by self-organization processes and by the substrate surface.[15−17] From the technologic point of view, the use of spin coating to fabricate polymer films for organic electronics is very attractive, as this technique combines simplicity, low cost, and versatility. The use of spin coating as a method to obtain patterned films of CPs at the micro and nanoscale has already been demonstrated in some studies. Arias et al. showed the optimization of organic photovoltaic cells and light-emitting diodes (LEDs) through the control of phase separation, from lateral to vertical, in cast films of blends of conjugated polymers.[18,19] In those systems, the modification to more viscous/less volatile solvents and the control of the phase separation kinetics allowed to obtain lamellar structures which proved to be beneficial in those devices, probably due to reduced leakage currents. In addition, a systematic study on the film morphology on spin-cast blends of various CPs (polyalkylthiophenes) and insulating polymers (PS) using different solvents showed a strong influence of the film morphology, from dewetted, lamellar or lateral, on the solubility parameters of the components in these ternary systems.[20] It is worth noting that, in contrast to polymer blends, spin-cast films of CPs (polydialkylfluorenes) and a soluble fullerene showed lamellar structures favored by lower solvent evaporation rates while films exhibiting lateral phase separation could be obtained by rapid film drying. On those particular systems, the low solubility limit and slow kinetics of crystallization of the fullerene component in the tested solvents is suggested to allow the system to be quenched into a metastable two-phase liquid−liquid region, originating lateral segregation of the blend components.[21]Recently, Castro et al.[22,23] reported on the fabrication of films of poly [2-methoxy-5-(2′-ethyl)hexyloxy-2,4-phenylenevinylene], MEH-PPV, with a nanostructured surface, through polymer demixing in spin-cast

*Corresponding author. E-mail: ana.charas@lx.it.pt.

Published on Web 09/25/2009

films of blends of MEH-PPV and polystyrene (PS) deposited on poly(3,4-ethylenedioxythiophene) doped with poly(styrenesulfonic acid) (PEDOT:PSS) covered substrates, followed by removal of PS with a selective solvent. In turn, Holdcroft et al. demonstrated the fabrication of nano/microscale patterned films of polythiophenes bearing solubilizing and thermally cleavable groups (tertrahydropyranyl, THP), also making use of phase separation during spin-casting polymer blends of the electroactive polymer and a dielectric polymer (poly(methyl methacrylate) or PS).[24] In this case, the thermal elimination of THP groups in acidic medium enables the dielectric polymer to be washed away leaving an insoluble dot matrix of conjugated polymer.[24] We note that surface pattern-ordered phase separation was also already reported in spin-cast blends of CPs and PSs deposited on chemically patterned surfaces, representing a step forward in relation to the isotropic patterning approach, although more complicated procedures are involved.[7,25]

The extension of patterning methods to produce insoluble films is particularly advantageous once additional layers may be deposited from solution. Here, we report on a similar approach to that first reported by Castro et al.,[22,23] using monodisperse PS as an assisting/insulating polymer, to fabricate insoluble patterns of cross-linkable CPs. Cross-linkable conjugated polymers have been prepared through the insertion of reactive groups (acrylates or oxetanes) at the end of flexible side groups of the conjugated backbone. Upon a photoinitiated reaction between these side groups, an insoluble polymer network is obtained, without affecting noticeably the optoelectronic properties of the CP.[26−29] In particular, in a previous work, we showed that the optical and electrochemical properties of polyfluorenes containing oxetane side groups are not significantly affected upon cross-linking.[30] We also demonstrated the optimization of LEDs, by the inclusion of a cross-linked layer of a polyfluorene derivative,[30] and field-effect transistors (FETs) based on cross-linked CPs.[31]

The development of insoluble patterned films is a three-step process: films of CP/PS blends are prepared by spin coating from toluene solutions, leading to the expected phase separation; in a second step, the CP is cross-linked forming an insoluble CP network. Finally, PS is removed using an adequate solvent, leaving behind a polymer network which is solvent-resistant. Our study is mainly focused on a cross-linkable derivative of poly(9,9-dioctylfluorene-*alt*-bithiophene), F8T2, referred as F8T2Ox2 (Scheme 1).

F8T2 has been extensively applied as a p-type channel in FETs showing good stability against light and air and mobility up to 10^{-2} cm^2/V s when an alignment substrate is employed to order the polymer chains parallel to the transport direction.[32,33] Recently, Bradley's group reported on the combination of effective charge transport with emission properties of F8T2, opening prospects for organic light-emitting FETs and electrically pumped organic lasers.[34] F8T2Ox2 structure differs from that of F8T2 by having two side chains containing cross-linkable oxetane end-groups instead of *n*-octyl side chains. The oxetane groups will polymerize via cationic ring-opening and form acyclic ether bonds leading to an insoluble polymer network. Insoluble films of cross-linked F8T2Ox2 can be prepared by depositing a solution of the polymer containing a catalytic amount of a photoacid generator (PAG) followed by UV illumination and annealing of the film.[28−31] We tailor film morphologies, pattern dimensions and film thicknesses by varying the experimental parameters controlling phase separation during spin coating, such as the CP:PS ratio, PS molecular weight, concentration of the blend solutions and spinning velocity. The CP is insolubilized by exposing the film to UV light and heat. PS is then removed by dissolution. This method, due to its simplicity, is a valuable tool to pattern CPs at small dimensions and large scales, especially when the integrity of the film against dissolution is required. It can be applied to fabricate multilayer devices with increased contact area between layers, such as multilayer LEDs or interpenetrating donor/acceptor systems for organic photovoltaic cells, OPVs, and tandem cells. Other applications, such as solid state chemosensors of enhanced active area are also envisaged if CPs incorporate specific functionalities.

Scheme 1. Synthetic Route to F8T2Ox2

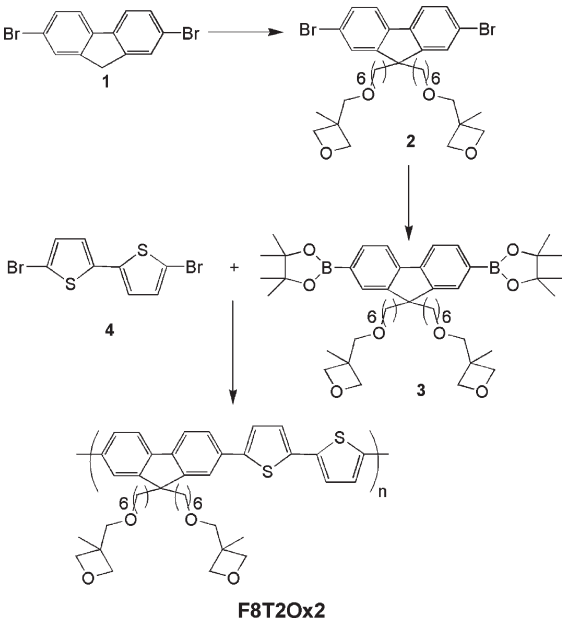

2. Results and Discussion

2.1. Synthesis and Properties of F8T2Ox2. F8T2Ox2 was prepared via the Suzuki coupling-type polymerization reaction (Scheme 1) with M_n = 8500 and M_w = 17000 as determined by Gel Permeation Chromatography against monodisperse polystyrene standards. F8T2 (M_n = 22400 and M_w = 38500), as a reference (non-cross-linkable) polymer, was prepared similarly. The cationic polymerization of the oxetane groups of F8T2Ox2 was promoted using a photoacid generator (PAG) ({4-[(2-hydroxytetradecyl)-oxyl]phenyl}phenyliodonium hexafluorantimonate}) which produces H^+, under UV light, acting as initiator for the ring-opening reaction.[30] Hence, cross-linked films of F8T2Ox2 were obtained by irradiating the spin-cast films prepared from toluene solutions of F8T2Ox2 containing 0.5% (by weight) of PAG, at 254 nm, for 1 min, at ca. 100 °C, followed by additional heating, for 5 min at the same temperature, under ambient atmosphere. High cross-linking yield is achieved under these conditions. The films were then rinsed with tetrahydrofuran, to remove any remaining soluble material and PAG. At the end of this procedure, the remaining films were completely insoluble in organic solvents and in water. Figure 1 shows absorption and emission spectra of F8T2Ox2 films both in the soluble and in the cross-linked forms. For comparison, F8T2 spectra are also shown, being similar to those reported in the literature.[35] The three absorption spectra are very similar. They show analogous optical gaps (2.3 eV for F8T2Ox2; 2.4 eV for F8T2), as deduced from the absorption onset. The maximum of the emission (or photoluminescence, PL) spectrum of F8T2 (occurring at 553 nm) is blue-shifted when compared to the spectra of F8T2Ox2, this shift being more pronounced for F8T2Ox2 in the cross-linked form (maximum at 585 nm). Such differences are probably related to the presence of

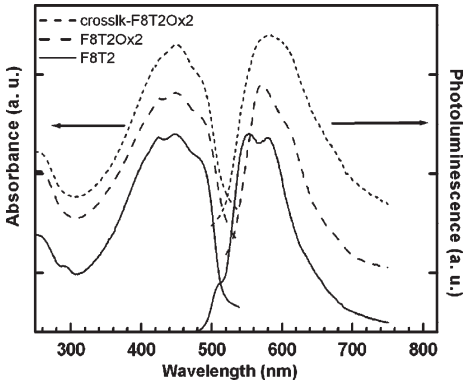

Figure 1. Normalized absorbance and photoluminescence spectra (excitation at 455 nm) of spin-cast films of neat F8T2Ox2 before and after cross-linking. For comparison, the F8T2 spectra are also shown. All the films are ca. 100 nm thick. Spectra were vertically shifted for better visualization.

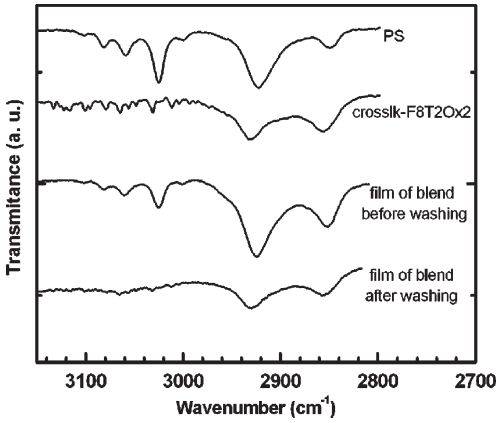

Figure 2. FTIR spectra of films prepared from a solution of (i) polystyrene, (ii) cross-linked F8T2Ox2, and (iii) a blend of F8T2Ox2 and PS, before and after washing with THF, spin coated onto PEDOT:PSS coated quartz substrates. A bare quartz substrate was used as the baseline.

oxetane groups and the effect of their polymerization which may affect chain packing and ordering in the solid state. A lower self-absorption may also contribute to the observed differences in PL, in the case of F8T2, as a small shoulder at 510 nm is observed in the PL spectrum.

The ionization potential (IP) and electron affinity (EA) of F8T2 and F8T2Ox2, in the soluble and in the cross-linked forms, were determined using cyclic voltammetry.[36] The measurements were performed on films drop cast onto a platinum substrate, functioning as the working electrode. The estimated values for F8T2 (IP = 5.5 eV; EA = 2.6 eV) compare well with the values found in the literature.[35] Minor differences were found for IP and EA of F8T2Ox2 in the soluble (IP = 5.3 eV; EA = 2.6 eV) and cross-linked forms (IP = 5.3 eV; EA = 2.7 eV), evidencing that the presence of the oxetane side groups and their polymerization has a negligible effect on these properties. However, hole mobilities, as determined using field-effect transistors (FETs), were shown to be much more sensitive to such structure modifications. In FETs using a SiO_2 dielectric treated with 1,1,1,3,3,3-hexamethyldisilazane, HMDS, the determined hole mobility for F8T2 is $\mu_h = 6.8 \times 10^{-3}$ cm^2/V s, which is similar to reported values.[32] In FETs using a SiO_2 dielectric we obtained $\mu_h = 1.7 \times 10^{-5}$ cm^2/V s for F8T2Ox2 and $\mu_h = 7 \times 10^{-6}$ cm^2/V s for cross-linked F8T2Ox2. A similar observation was previously reported using a slightly different cross-linkable polymer, F8T2Ox1, and was attributed to the disorder brought about by the presence of the polar oxetane side groups, which appears to be further emphasized upon cross-linking.[31] Nevertheless, these reduced values refer to nonoptimized structures; improved mobilities should, in principle, be achieved using strategies similar to those used to increase the mobility in F8T2.[33]

2.2. Patterned Films of Cross-Linked F8T2Ox2. Polymer blends solutions were prepared by dissolving monodisperse PS and F8T2Ox2 in toluene and adding a catalytic amount of PAG dissolved in THF. The solutions were then spin coated onto quartz substrates covered with a layer (ca. 50 nm thick) of PEDOT:PSS. PEDOT:PSS is widely used in LEDs and OPVs and was, therefore, selected as the substrate surface for this study. The spin-cast films were afterward cross-linked as described above and imaged by Atomic Force Microscopy, AFM. PS was then removed by immersing the films in THF under stirring, until complete disappearance of the PS absorption bands in the FTIR spectrum (at 3030, 3060, and 3090 cm^{-1} assigned to =C−H stretching vibrations) (Figure 2).

The surface topography of the remaining films was again imaged by AFM. We note that the patterned films may be removed from the quartz substrate by simply immersing the samples in water, which readily dissolves the PEDOT:PSS layer without destroying the patterned film and permits the transfer of the latter to another substrate by contact adhesion. This feature may be specially helpful to use the patterned films in other applications requiring substrates different from those used in this study.

We investigated the morphologies of the films obtained by varying the following: (i) molecular weight of PS, (ii) CP/PS ratio, (iii) concentration of blend solution, and (iv) spinning velocity.

2.2.1. Columnar-Grained and Spike Structured Films. Figure 3 shows AFM topographic (columns a and c) and phase images (columns b and d) of cross-linked F8T2Ox2/PS films, before and after PS removal, prepared from blends with different PS molecular weights (M_w = 500, 2×10^3, 2×10^4 and 1×10^5). For all the blends, the CP:PS ratio was 1:1 (by weight), the total concentration of polymeric materials (C) in the toluene solution was 26 mg/mL and the spinning velocity was 1750 rpm (ω_1) for 45 s. For comparison, an AFM topography image of a cross-linked F8T2Ox2:PS2000 film prepared under the same conditions but onto a bare quartz substrate (without PEDOT:PSS), after PS removal, is shown in Figure 3f. Figure 3g shows the topography of a spin-cast film of cross-linked, pure F8T2Ox2, deposited onto a PEDOT:PSS covered substrate.

Figures 3a−d evidence the effect of the PS removal and of its molecular weight on the surface topography of the films, in particular on the size of the columnar domains. The topography of the cross-linked films of the blends before PS removal consists on elevated domains that lie above a lower surface level. The dimensions of the domains increase with increasing PS molecular weight. After PS removal, a very well-defined columnar structure is revealed, with increased domain heights but lower film thicknesses (Figure 4 and Table 1). In our study, for simplicity, the designation "film thickness" stands for the whole vertical extension of the CP layer (perpendicular to the substrate surface). We estimated average film thicknesses from AFM measurements; for that, several scratches were made onto the films, the AFM tip was aligned with respect to each scratch, and the films were imaged. The film thickness corresponds to the height difference between the quartz substrates surface exposed by the scratch and the maximum height of the

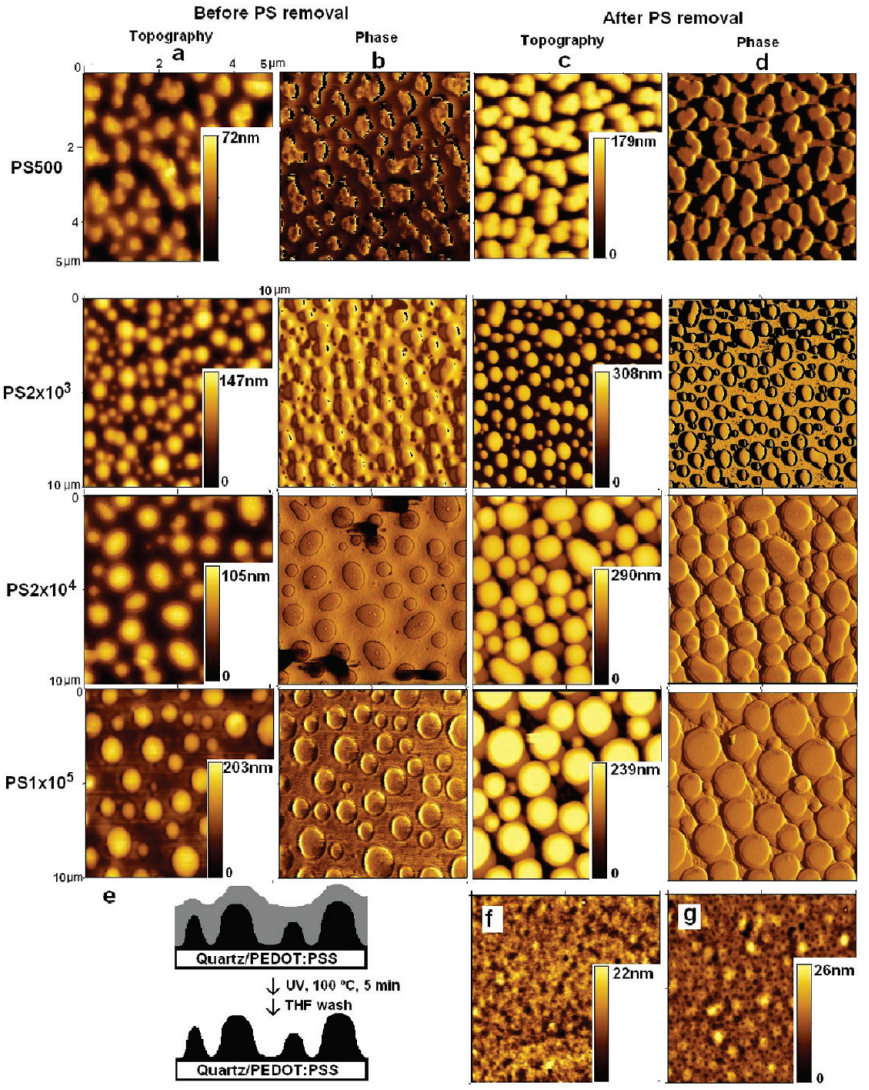

Figure 3. (a−d) AFM surface images of cross-linked films prepared from F8T2Ox2:PS (1:1) blends (26 mg/mL) in toluene, at spinning velocity ω_1 (1750 rpm), using different PS molecular weights, onto PEDOT:PSS coated quartz substrates. All the images have 10 μm × 10 μm dimensions, except those for blends prepared from PS500 (images in the first row) which are 5 μm × 5 μm, for better visualization. Topography and phase images, before and after PS removal, are shown. (e) Scheme of the films cross-section after polymers demixing and after PS removal (F8T2Ox2-phase in black and PS-phase in gray). (f) AFM topographic image of a cross-linked film obtained from a F8T2Ox2:PS2 × 10^3 blend prepared under identical conditions, spin-cast onto a bare quartz substrate. (g) AFM topography image of a cross-linked F8T2Ox2 pure film, after rinsing with THF.

surface motifs, averaged over several positions, after subtracting the PEDOT:PSS layer thickness. The latter was also determined by AFM, using PEDOT:PSS covered quartz substrates.

Average domain heights were determined using several surface profiles in 10 μm × 10 μm AFM images and measuring the peak-to-valley height distances. In cases where domain sizes were smaller, 3 μm × 3 μm or 5 μm × 5 μm images were considered. For comparison Figure 3g also shows the AFM topography image of a film obtained from a solution containing only F8T2Ox2 and PAG, spin-cast onto a PEDOT:PSS covered quartz substrate. For this case a thick film (thickness = 100 ± 15 nm) with a root-mean-square roughness of 4 nm was obtained.

From these results we conclude that, upon spin coating and cross-linking, PS forms an over layer, covering a CP-rich columnar-grain layer (part e in Figure 3). Furthermore, as the average domain heights are smaller than the corresponding film thicknesses, we deduce that there is an underlying CP layer, covering the PEDOT:PSS surface and supporting the columnar structure (see Figure 3, Table 1, and Table 2 in the Supporting Information). Since there was no evidence of CP removal when washing the cross-linked films (the washing solution remained uncolored), we consider that the thickness reduction is due to the removal of the PS top layer. We note that, when films of the F8T2Ox2/PS blends were spin coated directly on the quartz substrate and cross-linked using the standard protocol (Figure 3f), the yellow color of the washing solutions indicated that some CP was being removed.

Table 1 shows the surface topography characteristics of some of the studied films, after PS removal, as a function of blend composition, total blend concentration, and spinning velocity. All the domains in the 10 μm × 10 μm image or, in case of small domains, in the 5 μm × 5 μm image, were included in this analysis. Domain areas are the projected areas. Since blends based on PS2 × 10^3, PS2 × 10^4, and PS1 × 10^5 produced, in general, columnar-grain films with circular cross-section, analogous to those shown in Figure 3, the maximum diameter of the domains was considered in this analysis. For blends prepared with PS500, as columnar grains are better described as cylinders with ribbon-type sections, as it is shown in Figure 3, two length scales were

considered: the longitudinal direction (L) and the width (W) (transversal length) of the domains sections.

Table 1 shows that the film thickness is reduced as PS molecular weight decreases (compare samples 1, 7, 9, and 10), as the total blend concentration decreases (compare for example samples 1, 2, and 3 and samples 10, 12, and 14), and as spinning velocity increases (compare for example samples 5 and 6, 10 and 11, or 12 and 13). The film final thickness is determined by a balance between centrifugal and viscous forces, acting in opposite trends, and related to spin velocity and solution viscosity, respectively.[37,38] Therefore, the reduction in thickness as the PS molecular weight decreases and the blend solutions get more diluted is interpreted as due to the lowering of the viscosity of the solutions. The reduction in thickness when the spinning velocity increases is related to larger centrifugal forces. In fact, the film thickness of the PS-free films (after removing PS) for symmetrical blends ($C_{CP} = C_{PS}$) prepared from PS500 and PS1 $\times$ 10^5, where a representative number of samples with different characteristics (concentration and spinning velocity) was investigated (data from Table 1 and Table 2 in the Supporting Information), scales linearly with $C_{CP}/\omega^{1/2}$ (Figure 5), in accordance to theoretical approaches[38,39] and similarly to results found for other polymer blend systems.[40,41] The higher linear coefficient found for the blend prepared with PS1 $\times$ 10^5 (779 $\pm$ 27 nm mL rpm$^{1/2}$/mg) compared with those estimated for the blends with PS500 (408 $\pm$ 22 nm mL rpm$^{1/2}$/mg) denotes that for blends from the high molecular weight PS yield thicker films. Such tendency of thickness growth with the increasing of PS molecular weight was also observed for a set of spin-cast PS solutions differing exclusively in the polymer molecular weight (thickness $\sim M_w^{1/4}$), thus describing the effect of the viscosity of the solution (solutions of PS of higher molecular weight are more viscous due to the lower diffusion coefficient of the solute) on the film thickness.[39]

Table 1 also shows a strong variation of the average domain areas. If we compare similarly prepared films, but obtained from blends using different PS molecular weights, (samples 1, 7, 9, and 10), domain areas increase by about 1 order of magnitude when PS molecular weight increases from 500 to 1 $\times$ 10^5, indicating an increasing tendency for phase separation. Domain sizes may also be affected by the CP:PS ratio. In particular, columnar section areas can be reduced by lowering the CP content of the blend solution (compare for example samples 12 and 16). Domain sizes are also larger for the films prepared at lower spinning velocity and from more concentrated blend solutions. The dependence of the film morphology on spinning velocity should be related to the solvent drying time; longer times for the solvent

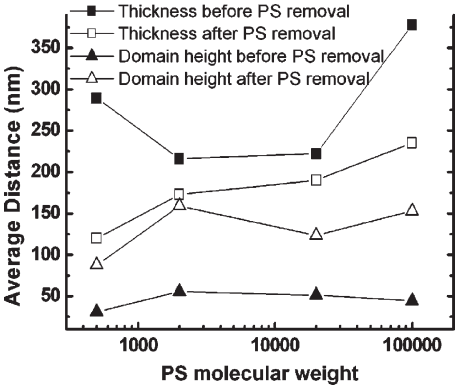

Figure 4. Averaged film thickness and domain height, before and after PS removal, as functions of PS molecular weight. The films were prepared from 1:1 blends, with the same total polymer concentration (26 mg/mL in toluene) and spinning velocity (ω_1, 1700 rpm). Lines are guides to the eye only.

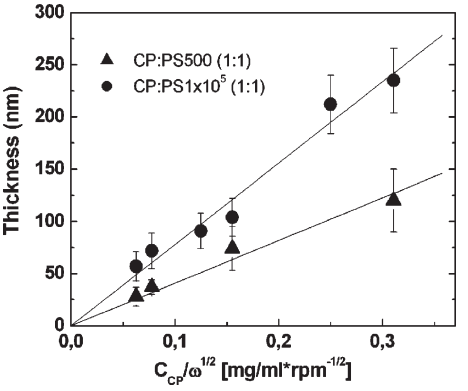

Figure 5. Film thickness (average values), measured after removing PS, of films prepared from symmetric (1:1) blends with PS500 and PS1 $\times$ 105 as a function of $C_{CP}/\omega^{1/2}$ ($= C_{PS}/\omega^{1/2}$). The solid lines represent the linear fits.

Table 1. Blends Characteristics, Average Thicknesses, and Feature Dimensions of the Films of Cross-Linked F8T2Ox2 (CP) after Removing PS[a]

sample	blend	CP:PS ratio (w/w)	concn	ω	thickness (nm)	av domain area (μm^2)	av domain height (nm)	av domain diameter (nm)
1	CP:PS500	1:1	C	ω_1	120 $\pm$ 30	0.2 $\pm$ 0.1	88 $\pm$ 37	596 $\pm$ 261 (L) 379 $\pm$ 161 (W)
2[b]		1:1	$^1/_2C$	ω_1	74 $\pm$ 21		58 $\pm$ 17	
3		1:1	$^1/_4C$	ω_1	37 $\pm$ 7	0.02 $\pm$ 0.01	12 $\pm$ 4	205 $\pm$ 124 (L) 111 $\pm$ 59 (W)
4[c]		3:1	C	ω_1	83 $\pm$ 20	0.04 $\pm$ 0.03[d]	68 $\pm$ 24[e]	280 $\pm$ 132[d]
5		1:2	$^1/_2C$	ω_1	102 $\pm$ 9	0.06 $\pm$ 0.05	32 $\pm$ 10	386 $\pm$ 354 (L) 199 $\pm$ 147 (W)
6		1:2	$^1/_2C$	ω_2	53 $\pm$ 8	0.02 $\pm$ 0.01	21 $\pm$ 7	152 $\pm$ 111 (L) 86 $\pm$ 62 (W)
7	CP:PS2$\times$10^3	1:1	C	ω_1	173 $\pm$ 40	0.3 $\pm$ 0.2	159 $\pm$ 51	630 $\pm$ 279
8[c]		2:1	C	ω_1	184 $\pm$ 35	0.4 $\pm$ 0.2[d]	117 $\pm$ 30[e]	818 $\pm$ 477[d]
9	CP:PS2$\times$10^4	1:1	C	ω_1	190 $\pm$ 27	0.8 $\pm$ 0.5	123 $\pm$ 48	1165 $\pm$ 419
10	CP:PS1$\times$10^5	1:1	C	ω_1	235 $\pm$ 31	1.2 $\pm$ 0.8	153 $\pm$ 58	1533 $\pm$ 745
11		1:1	C	ω_2	212 $\pm$ 28	0.3 $\pm$ 0.2	145 $\pm$ 49	707 $\pm$ 302
12		1:1	$^1/_2C$	ω_1	104 $\pm$ 18	0.2 $\pm$ 0.1	84 $\pm$ 18	604 $\pm$ 190
13		1:1	$^1/_2C$	ω_2	91 $\pm$ 17	0.14 $\pm$ 0.09	75 $\pm$ 17	491 $\pm$ 159
14		1:1	$^1/_4C$	ω_1	72 $\pm$ 17	0.10 $\pm$ 0.06	40 $\pm$ 9	414 $\pm$ 137
15		4:1	C	ω_1	192 $\pm$ 25	10 $\pm$ 8	106 $\pm$ 21	4338 $\pm$ 2266
16		1:3	$^1/_2C$	ω_1	94 $\pm$ 25	0.08 $\pm$ 0.08	81 $\pm$ 24	371 $\pm$ 193

[a] C = 26 mg/mL; ω_1 = 1750 rpm, 45 s; ω_2 = 2700 rpm, 45 s. [b] Bicontinuous morphology. [c] Porous film. [d] It refers to porous dimensions. [e] It refers to porous depth. L/W = longitudinal/width dimensions of the ribbon-type surfaces.

to evaporate, typically yield more developed phase separated structures.[40,41] The dependence of domain size on film thicknesses, also observed in several other systems, is interpreted on the basis of a thickness control on domain growth.[16,42] During film thinning due to solvent evaporation, at a certain point, the domains growth gets geometrically constrained; their sizes being limited by the thickness of the film. Support for this model in our system comes from the comparison between the average domain areas and the corresponding average film thicknesses, showing that domain areas are smaller for thinner films. Considering that final film morphologies correspond to frozen structures formed during solidification, we can infer that the initial phase separation process takes place in a surface-oriented fashion, forming a relatively thin layer of CP wetting the surface substrate (PEDOT:PSS), and evolves under a lateral demixing process with characteristics depending on the film thickness and, probably, on the solubility of the blend components. When spin-casting a solution of two polymers in a single solvent over a substrate, as the solvent evaporates, the system will go from a one-phase region of the ternary phase diagram (polymer/polymer/solvent) to a two-phase region, initiating the phase separation process. Phase separation proceeds as the solvent evaporates until the molecules of one of the polymer blend components loose their mobility. Some studies have suggested that a probable mechanism for lateral phase separation occurring during the spin coating of polymer blends from solution is the creation of a transient layered film, by a process of wetting followed by the breakup of the layers because of an interfacial instability.[17,43] The instabilities at the polymer−polymer interface leading to lateral demixing may arise from different circumstances. Heriot et al. suggested that the origin of those instabilities is the solvent concentration gradient due to the fast solvent evaporation on the film surface which can not be compensated by the solvent diffusion through its bulk.[43] Other authors,[16,17,37,44] stressed the importance of different solubilities of the two blend components, as the cause for such instabilities. According to this scenario, in a ternary system of two immiscible polymers, depending on their relative solubility in the common solvent, one of the polymer phases is depleted of the solvent quicker and solidifies first, forming domains enriched in the less soluble polymer. Subsequent evaporation leads to further solidification of the more soluble polymer forming a continuous phase. The system studied in this work is quasi-ternary, because F8T2Ox2 is not a monodisperse polymer (polydispersity (D) = 2). However, we refer to our blends as binary, since we do not expect a significant solubility variation across the molecular weight distribution. Furthermore, the solvent used is, in fact, a mixture of toluene and THF (PAG is dissolved in THF), but due to the small content of THF in the mixture ($\leq$10%), for simplicity, we consider the solvent to be toluene. Toluene dissolves PS faster than it dissolves F8T2Ox2. Therefore, we suggest that, in these blends, F8T2Ox2 is the less soluble component. Accordingly, the depletion of the F8T2Ox2-phase from the solvent should occur first, creating an F8T2Ox2-rich layer coating the PEDOT:PSS surface with elevated structures embedded in a PS phase still swollen with solvent. On the other hand, the PEDOT:PSS layer appears to play an important role in this phase separation process. The results shown in Figure 3-f support this conclusion. In fact, cross-linked films prepared from blends of F8T2Ox2 and PS2 $\times$ 10^3 on bare quartz substrates, using a similar procedure to that used for the preparation on PEDOT:PSS, are much thinner (81 $\pm$ 2 nm, compared to a thickness of 173 $\pm$ 24 nm for the corresponding film on PEDOT:PSS, sample 7 in Table 1 and image for PS2 $\times$ 10^3 in column c in Figure 3) and smoother, having a root-mean-square (r.m.s.) roughness of 2 nm, instead of a columnar-grain structure. This suggests that, on bare quartz, a vertically segregated film (lamellar structure) is produced. The higher film thickness observed on PEDOT:PSS is attributed to higher interactions with the substrate surface: in view of the acidic nature of PEDOT:PSS, some oxetane ring-opening reaction may be initiated leading to increased polar interactions between F8T2Ox2 and the PEDOT:PSS surface. We note that, in support of the role played by PEDOT:PSS in promoting the reticulation reaction, a noticeable amount of soluble F8T2Ox2 was washed out from films cross-linked onto bare quartz substrates.

We have also investigated the role of the annealing and the washing step in the film morphologies. Hence, we examined several films just after spin coating, before and after carrying out the cross-linking protocol and upon washing with different solvents to remove PS (to investigate possible swelling effects). However, no significant differences on the film morphologies were found. Thus, we conclude that final film morphologies are mostly due to phase separation occurring during the spin coating process. A columnar-grain structure elevated from an underlying layer represents the ideal film morphology for the electron donor in heterojunction photovoltaic applications, since when covered with the second active layer (the electron acceptor), no direct paths are established between the cathode and the anode.[23] Direct paths, formed when one or both components contact both electrodes in the cell, are undesirable, since they act as shunt resistance, lowering the open-circuit voltage.[45,46] Moreover, given the insolubility of the patterned film, further deposition of the acceptor may be carried out from solution. Still, ideally, columns cross section radius should approach the diffusion length for photoexcitons generated on the polymer, otherwise they can be trapped and/or decay before attaining the interface with the second active component, not contributing to charge generation. The exciton diffusion length in conjugated polymers has been determined as ca. 10 nm,[47,48] meaning that the optimal column cross section diameters should be less than 20 nm. With a view to reaching those dimensions, while maintaining reasonable film thicknesses and column heights, we carried out several additional studies. We managed to reduce the domain area until their length scale fell into the range of 100 nm (sample 6 in Table 1). As it is shown by the AFM profile measurements (Figure 6a), these morphologies exhibit sharp edges (spike structures).

On the basis of the above dependences, we can establish some strategies to tailor feature dimensions and film thicknesses. For instance: (i) the effect of higher fluid viscosity in blends with higher molecular weight PS on the increase of film thickness and domain size, can be compensated by using higher spinning velocities or lower blend concentration; (ii) domain sizes can also be reduced by increasing PS content. These approaches are illustrated in Figure 6b, for CP:PS1 $\times$ 10^5 (1:1) blends (or samples 10, 11, 12 and 14).

2.2.2. Porous Films. Functional porous films of conjugated polymers may lead to new efficient devices with applications ranging from solid state sensors[49] to heterogeneous catalysts,[50] etc. Insoluble scaffold-type morphologies (porous films) could be obtained upon increasing CP content (see sample 6 and 8 in Table 1) in blends with PS500 and PS2 $\times$ 10^3 (after removing PS) (Figure 7).

These structures are formed by merging F8T2Ox2 domains into a continuous phase, with PS forming isolated

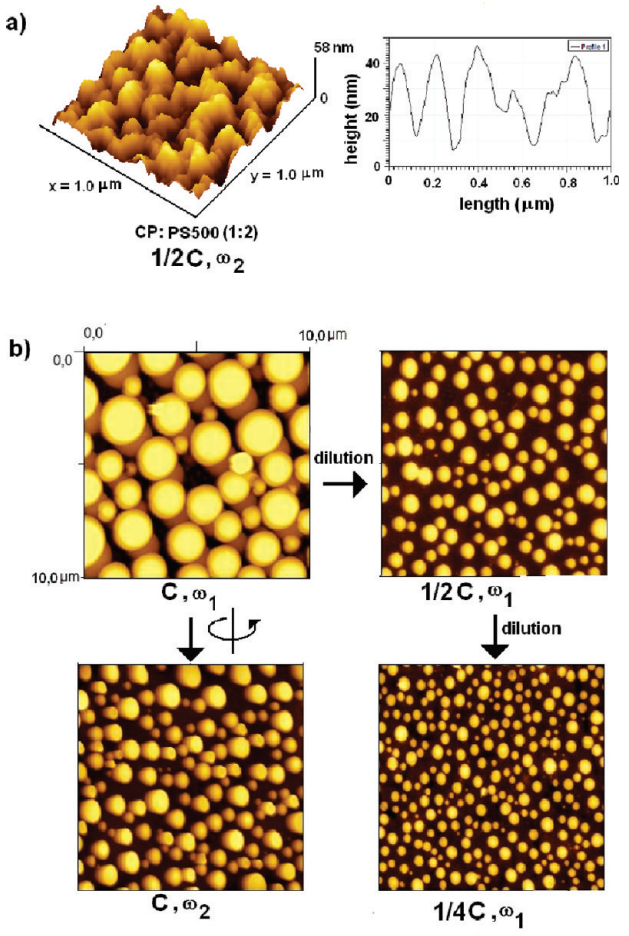

Figure 6. (a) AFM topography image (1 μm × 1 μm) showing a spike structured film and sectional view along a line in the AFM image (sample 6 in Table 1); (b) AFM topography images of cross-linked F8T2Ox2 films (after PS removal) prepared from blends with PS1 × 10^5 (1:1) showing surface morphology modifications by varying the concentration and the spinning velocity (C = 26 mg/mL, ω_1 = 1730 rpm; ω_2 = 2700 rpm).

domains. In fact, we observe that for a lower PS content, smaller porous are obtained, as it is shown in Figure 7. Still, for high molecular weight PS (PS1 × 10^5) the increase of CP content leads to an increase of domain size but no porous films were obtained, even for a 4CP:1PS composition (sample 15 in Table 1). This tendency for CP domains to grow, instead of merging, may be related to a less effective PS transport to regions of lower concentration, due to the lower diffusivity of the higher molecular weight PS chains.

2.3. Patterning Other Cross-Linkable Conjugated Polymers. In order to test the application of this patterning method to other cross-linkable CPs, we investigated blends of polystyrenes with two other cross-linkable luminescent polymers, namely, F8T2Ox1[31] (structurally analogous to F8T2Ox2 but containing only one cross-linkable oxetane group per repeat unit) and the blue-emitter F8Ox (poly[2,7-(9,9-dioctylfluorene)-*alt*-1,4-(2,5-bis(methyl-4-(6-(3-methyl-oxetan-3-yl)methoxy)hexyloxy)benzene]).[30] As both polymers are cross-linkable under analogous conditions to those used for F8T2Ox2, similar protocols were followed to prepare patterned films. Figure 8 shows two AFM topographic images (after PS removal) obtained for films prepared by spin coating F8T2Ox1/PS2×10^4 and F8Ox/PS2×10^4 blends onto quartz/PEDOT:PSS substrates. For these systems, several blends were investigated, using toluene as solvent.

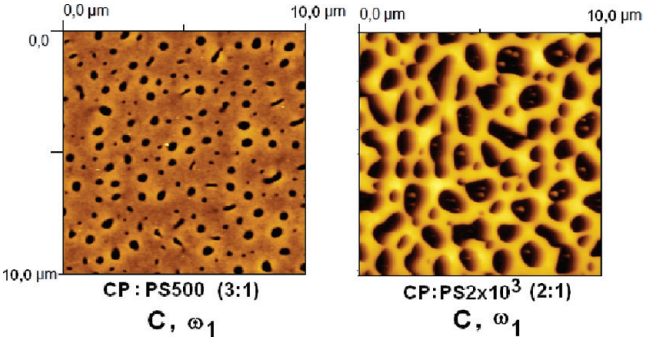

Figure 7. AFM topographic images showing porous films of F8T2Ox2 obtained upon increasing F8T2Ox2 content in its blends with PS. Films were prepared with the same blend concentration and spinning velocity.

In contrast with the results obtained with F8T2Ox2, when PS500 was blended with these two CPs, F8T2Ox1 and F8Ox, smooth films (rms < 3 nm) were obtained (after PS removal). In these cases, phase separation apparently yields almost lamellar morphologies, indicating a strong dependence of the film morphology on PS molecular weight. Strong variations with PS molecular weight were also observed for spin-cast films prepared from blends of PS and doped polyaniline.[51] Castro et al.[22] also observed lower surface structuring in AFM images of films prepared from MEH-PPV and lower molecular weight PS. These authors explained these dependences in terms of stronger influences of the substrate surface on the phase separation process for thinner films, which are produced when lower molecular weight PS is used. Indeed, for F8T2Ox1 and F8Ox we actually observe a strong reduction of film thickness and, simultaneously, a strong dependence of the film morphology upon using PS of low molecular weight: films prepared similarly from F8T2Ox1/PS2×10^4 and F8Ox/PS2×10^4 blends are 155 ± 18 nm and 117 ± 11 nm thick respectively, while from the corresponding blends with PS500, films with thicknesses of 64 ± 21 nm and 54 ± 17 nm, respectively, were obtained. We expect that the same general strategies investigated for F8T2Ox2 can be used to tune the morphologies of the films based on these two CPs, so a complete study will be carried out.

2.4. Donor−Acceptor Columnar Bilayers. In order to assess potential applications of the prepared columnar-grain films in donor−acceptor bilayers as active layers for OPV cells, we determined the polymer emission quenching in donor−acceptor columnar bilayers. The polymer emission quenching in polymer−fullerene systems is generally used to evaluate the efficiency of the excited state charge transfer between the two components.[52,53] The columnar bilayer films were prepared by depositing a chlorobenzene solution (3%, wt/wt) of 1-(3-methoxycarbonyl)propyl-1-phenyl-(6,6)C_{61} (PCBM), by spin coating, on top of columnar-grain films of cross-linked F8T2Ox1, prepared following the protocol here described. PCBM being a soluble fullerene derivative has been widely used in donor−acceptor systems in efficient OPV cells (efficiency ca. 3−5%) where the electron donor is a p-type conjugated polymer.[54−56] Comparing the IP and EA estimated for F8T2Ox1 after cross-linking, 5.41 and 2.65 eV respectively,[31] with the same properties for PCBM (IP = 6.1 eV and EA = 3.75 eV, respectively)[52] we predict energetically favorable electron transfer from the photoexcited polymer to PCBM. Hence, we prepared bilayers from two types of structures: columnar-grain films whose topography is shown in Figure 8 (left image) and from thinner columnar-grain film (film thickness = 123 ± 23 nm)

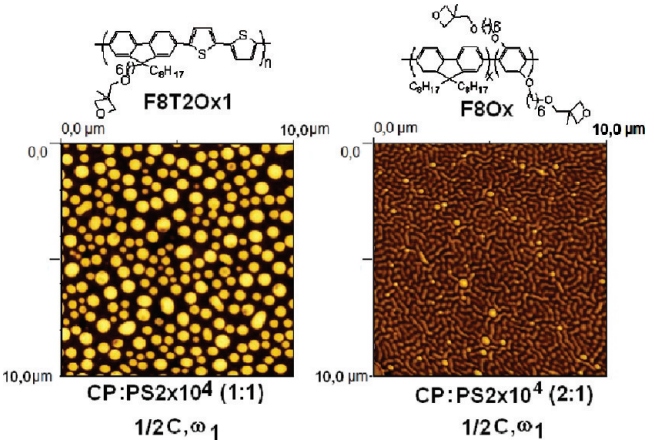

Figure 8. Structure of F8T2Ox1 and F8Ox and respective AFM topographic images of spin-cast films, after removing PS, prepared from blends with PS2×10^4. Left image: the film thickness is 155 ± 17 nm, the average domain diameter is 457 ± 134 nm and the average domain height is 81 ± 16 nm. Right image: the film thickness is 117 ± 11 nm, the average domain diameters are 451 ± 303 nm (length) and 214 ± 134 nm (width), and the average domain height is 20 ± 6 nm.

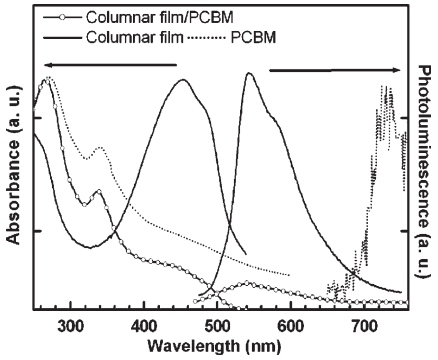

Figure 9. Normalized absorbance and photoluminescence spectra (λ_{exc} = 450 nm) of a columnar-grain film of cross-linked F8T2Ox1 and of a spin-cast PCBM film. The emission spectrum intensity of the columnar bilayer film (line with circles) is 10% of that obtained for the neat F8T2Ox1 film.

with shorter and narrower columns (average column height = 28 ± 8 nm; average domain diameter = 356 ± 84 nm) and compared the intensity of the polymer emission band, before and after depositing PCBM. We have obtained a 90% PL quenching for the bilayers prepared from films with the wider columns and a 95% PL quenching for the thinner films with narrower columns. Figure 9 shows the absorption and emission spectra for the 90% case. When going to the 95% case, the spectra are analogous in shape. These high values for the polymer emission reduction upon PCBM deposition suggest that photoinduced charge transfer may be an efficient process in these structures.

To evaluate the benefit of using the columnar bilayers prepared from cross-linked donor components, we investigated planar bilayer structures combining a "flat" layer of the noncross-linkable polymer F8T2 (rms ~ 2 nm) where PCBM was thermally evaporated on top (~100 nm thick). As referred above, the IP and EA for F8T2 and for F8T2Ox1 are approximately the same (see section 2.1). However, in these planar bilayers only PL reduction of 33% was observed. Considering that the columnar-grain films exhibit a 10−30% of increased surface area if compared with "flat" substrates, the PL quenching values found for the columnar bilayer films are extremely high. Further studies and time-resolved emission experiments are in progress to investigate the dynamics of the excited states in these systems.

3. Conclusions

A rich variety of film morphologies is obtained by spin coating blends of a cross-linkable conjugated polymer and polystyrenes. Patterned films of insoluble cross-linked CPs with feature dimensions at the submicrometer range were prepared onto PEDOT:PSS covered substrates. We conclude that the phase separation process occurring during spin coating proceeds via a surface-oriented fashion forming a layer of CP wetting the substrate surface, and evolves under a lateral demixing process probably affected by film thickness evolution and blend components solubility. In particular, this study demonstrated that the preparation of patterned films using the phase separation during the spin coating of blends with PS can be extended to cross-linking conjugated polymers to obtain columnar-grain structures, spiked structures and porous films. Feature dimensions can be tuned by controlling the blend characteristics and the spinning velocity. Applications to other cross-linkable conjugated polymers demonstrates the versatility of this patterning method for the fabrication of structured films for various optoelectronic applications. Evidence of efficient PL quenching in donor−acceptor columnar bilayers using a cross-linked conjugated polymer as donor suggest efficient exciton dissociation in those structures and open prospects for applications in PV cells.

4. Experimental Section

Materials and Synthesis. The palladium(0) tetrakis-(triphenylphosphine) catalyst was purchased from Aldrich and handled under inert atmosphere. The tetraethylammonium hydroxide (Et_4NOH) used in the polymerization reactions was purchased from Aldrich as aqueous solution (20%). 2,7-dibromofluorene (**1**) and 5,5′-dibromo-2,2′-bithiophene were purchased from Aldrich and used as received. All solvents used for synthesis were purified according to standard methods. All reactions were carried out under inert atmosphere (N_2).

2,7-Dibromo-9,9-bis-[methyl-4′-(6-(3-methyloxetan-3-yl)-methoxy)hexyl]fluorene (2). A 1.94 g (6 mmol) sample of 2,7-dibromofluorene was added to a solution of 20 mL of NaOH-(aq) (50%) containing 0.65 g (2 mmol) of tetrabutylammonium bromide, under stirring, at room temperature. The suspension was warmed to 60 °C for 15 min and 3-(6-bromo-2-oxahexyl)-3-methyloxetane[57] (3.98 g, 15 mmol) was added under N_2, dropwise. The reaction was allowed to proceed at 60 °C for 24 h. The product was extracted with a mixture of THF/Et_2O (50:50, v/v) several times and the organic phase was washed with H_2O until neutral pH, and dried with Na_2SO_4. After evaporation of the solvent, a red oil was obtained. The excess of 3-(6-bromo-2-oxahexyl)-3-methyloxetane was removed by distillation under vacuum and the product was separated as a pale yellow oil by column chromatography on SiO_2 using petroleum ether/EtOAc (7/3, v/v) as eluent. Yield: 84%. Anal. Calcd for $C_{35}H_{48}Br_2O_4$: C, 60.70; H, 6.98. Found: C, 60.75; H, 7.30. ^{1}H NMR (300 MHz, $CDCl_3$), δ (ppm): 7.52−7.44 (6H, m); 4.48−4.46 (4H, d, J = 5.7 Hz); 4.34−4.32 (4H, d, J = 5.7 Hz); 3.41 (4H, s); 3.36−3.32 (4H, t, J = 6.6 Hz); 1.94−1.89 (4H, m); 1.41−1.37 (4H, m); 1.27 (6H, s); 1.10−1.08 (8H, m); 0.61−0.55 (4H, m). ^{13}C NMR (75 MHz, $CDCl_3$): 152.16; 138.84; 130.02; 125.89; 121.32; 121.01; 79.93; 75.76; 71.23; 55.40; 39.90; 39.62; 29.44; 29.17; 25.52; 23.38; 21.20.

2,7-Bis(4,4,5,5-tetramethyl-1,3,2-dioxaborolan-2-yl)-9,9-bis-[methyl-4′-(6-(3-methyloxetan-3-yl)methoxy)hexyl]fluorene (3). To a solution of 1.32 g (1.9 mmol) of (**2**) in 15 mL of tetrahydrofuran, under stirring, at −78 °C was added 4.9 mL of *tert*-BuLi (1.7 M in pentane) dropwise, under N_2. After 2 h at −78 °C, the reddish suspension was warmed to 0 °C for 15 min and then cooled again to −78 °C. At this temperature,

1.44 g (7.6 mmol) of 2-isopropoxy-4,4,5,5-tetramethyl-1,3,2-dioxaborolan was added under N_2 and the reaction was allowed to warm until room temperature and stirred for 24 h. After this period, 10 mL of H_2O were added and the phases were separated. The aqueous phase was extracted with Et_2O, the extracts were collected and the organic phase was washed with brine and dried over Na_2SO_4. After evaporation of the solvent, a colorless oil which slowly crystallized at 0 °C was obtained. Recrystallization in *n*-pentane yielded the pure product as a white solid. Yield: 85%. Anal. Calcd for $C_{47}H_{72}B_2O_8$: C, 71.76; H, 9.22; Found: C, 71.27; H, 9.02. ^{1}H NMR (300 MHz, $CDCl_3$), δ (ppm): 7.82−7.79 (2H, d, J = 7.5 Hz), 7.71 (2H, s), 7.71−7.69 (2H, d, J = 7.5 Hz), 4.44−4.42 (4H, d, J = 5.7 Hz); 4.30−4.28 (4H, d, J = 5.7 Hz); 3.37 (4H, s); 3.32−3.28 (4H, t, J = 6.6 Hz); 1.95 (4H, m); 1.39−1.24 (10H, br); 1.04 (8H, m); 0.61−0.55 (4H, m). ^{13}C NMR (75 MHz, $CDCl_3$): 150.26; 143.87; 133.69; 128.77; 119.40; 83.73; 80.24; 75.98; 71.53; 55.08; 40.14; 39.79; 29.81; 29.42; 25.73; 24.92; 21.33.

F8T2Ox2. The polymerization reaction was carried out in a refluxing toluene/aqueous Et_4NOH (20%) degassed mixture (30 mL of toluene/15 mL of aqueous solution), containing 2.4 mmol of 5,5′-dibromo-2,2′-bithiophene and 2.4 mmol of (**3**) and $Pd(PPh_3)_4$ (2% mol) for 48 h, in the dark, under N_2 and vigorous stirring. The product was precipitated by addition of the reaction mixture to 250 mL of methanol under stirring. The collected solid was dissolved in toluene and the solution was filtered and stirred overnight with aqueous NaCN solution (1%, w/w) overnight. The phases were separated and the organic phase was washed with water and concentrated by removing the solvent under reduced pressure. The product was precipitated in methanol, collected by filtration, washed with methanol in a Soxhlet extractor and dried overnight under dynamic vacuum. Yield: 58%. Anal. Calcd for $C_{43}H_{52}O_4S_2$: C, 74.10; H, 7.52; S, 9.20. Found: C, 73.07; H, 8.54; S, 10.09. M_n = 8500, M_w = 16700, M_w/M_n = 2.0. IR (KBr pellet, cm^{-1}): 2920 (CH_2), 2850 (CH), 1460 (C=C), 1110 (C−O−C acyclic), 980 (C−O−C oxetane), 790 (C−S). ^{1}H NMR (300 MHz, $CDCl_3$), δ (ppm): 7.70−7.57 (6H, m); 7.35−7.20 (4H, m); 4.44−4.42 (4H, d, J = 5.7 Hz); 4.30−4.28 (4H, d, J = 5.7 Hz); 3.37 (4H, s) 3.31 (4H, br), 2.04 (4H, m); 1.38 (4H, m); 1.25 (6H, s); 1.11 (8H, m); 0.69 (4H, m). ^{13}C NMR ($CDCl_3$): 151.58; 143.66; 140.30; 136.45; 132.93; 127.89; 124.63; 123.71; 120.24; 119.58; 80.17; 77.20; 75.92; 71.48; 55.25; 40.39; 39.76; 29.68; 29.36; 25.68; 23.67; 21.31.

Characterization Techniques. FT-IR spectra were recorded using a Mattson 1000 spectrophotometer. Number-average (M_n) and weight-average (M_w) molecular weights were estimated by gel permeation chromatography (GPC) in a Waters 51 chromatograph equipped with two Waters UltraStyragel columns (1000 Å-500 Å) in series and with two detectors (a Water 410 differential refractometer and a scanning fluorescence detector) at a flux rate of 1 mL/min. GPC analysis were performed on filtered solutions (0.45 μm, Millipore Millex HV) of the copolymers in tetrahydrofuran (THF) and using polystyrene standards. UV/vis absorption spectra were recorded in a Cecil 7200 spectrofotometer. Fluorescence spectra were acquired in a SPEX Fluorolog 19340 spectrophotometer with an integrated sphere as the sampler. Ionization potential and electron affinity values were estimated from cyclic voltammetry (CV), in a Solartron potentiostat using tetrabutylammonium tetrafluorborate/CH_3CN supporting electrolyte, at a scan rate of 50 mV/s. A saturated calomel reference electrode (SCE), calibrated against ferrocene, Fc/Fc^+ (0.42 V), a platinum wire as counter electrode and a platinum disk as working electrode were used. As the energy level of Fc/Fc^+ is estimated to lie at 4.8 eV below the vacuum level[58] we calculate IP (eV) = $E_{onset,ox}$ (eV) + 4.38 and EA (eV) = $E_{onset,red}$ (eV) + 4.38. Atomic force microscopy (AFM) measurements were performed on a Molecular Imaging (model 5100) system operating in noncontact mode (at a resonance frequency between 200 and 400 kHz) using silicon probes with tip radii lower than 10 nm. All images were taken with 250 × 250 pixels resolution and were processed using the same leveling procedure with the final images indicating a flat planar profile, as expected. Gwyddion (version 2.9) software was used to process the images.

FETs Fabrication. FETs of the bottom gate, top contact type structure were prepared on a n^{+2}-Si/SiO_2 (625 nm, thick) substrate. The SiO_2 surface was cleaned with 2-propanol (HPLC grade) in a ultrasonic bath prior to the deposition of the F8T2Ox2 solution containing a 0.5% (by weight) of PAG by spin coating. After implementation of the cross-linking protocol gold source and drain contacts were thermally deposited on top of the cross-linked film, using a shadow mask to define the channel (length = 120 μm, width = 5.1 mm). Devices were tested in air.

Patterned Films Preparation. Quartz substrates were cleaned in an aqueous H_2SO_4/H_2O_2. (7%) mixture followed by rinsing with distilled water and drying under a nitrogen flow. They were treated with oxygen plasma prior to PEDOT:PSS (Bayer, Baytron P) deposition by spin coating. These films were dried on a hot plate for 10 min at about 100 °C. Solutions of F8T2Ox2 (26 mg/mL) and polystyrene GPC standards from Fluka (with molecular weights of 500, 2×10^3, 2×10^5, and 1×10^5) (26 and 52 mg/mL) were prepared in toluene. The photoacid generator (PAG) {4-[(2-hydroxytetradecyl)oxyl]phenyl}phenyliodonium hexafluorantimonate (Aldrich) solution (6 mg/mL) was prepared in THF and kept under dark conditions. Polymer blend solutions were prepared by mixing the adequate volumes of polymer and PAG solutions. The solutions were stirred overnight and filtered (0.2 μm, Millipore Millex HV) before being spin-casting onto PEDOT:PSS coated quartz substrates. Cross-linking of the films was promoted by exposing the samples at about 100 °C, on a hot plate, to a 4 W UV light (254 nm) for 1 min followed by an additional heating period of 5 min. The obtained films were imaged by AFM. Afterward they were washed twice in stirred baths of fresh THF to remove PS. The cross-linked, PS free, films were characterized by FTIR spectroscopy and AFM. Reference films of the pure polymer, F8T2Ox2, both in the soluble form and in the cross-linked form, were also prepared onto PEDOT:PSS covered quartz substrate and investigated by FTIR, UV−vis absorption, fluorescence spectrofotometry, and AFM.

Acknowledgment. This work was partially financed by FCT-Portugal (contracts no. PTDC/FIS/72831/2006 and PTDC/CTM/64127/2006).

Supporting Information Available: Table 2 showing thicknesses and feature dimensions of patterned films of F8T2Ox2 after removing PS prepared under other conditions. This material is available free of charge via the Internet at http://pubs.acs.org.

References and Notes

(1) Holdcroft, S. *Adv. Mater.* **2001**, *13*, 1753.
(2) Nie, A.; Kumacheva, E. *Nat. Mater.* **2008**, *7*, 277.
(3) Pardo, D. A.; Jabbour, G. E.; Peyghambarian, N. *Adv. Mater.* **2000**, *12*, 1249.
(4) de Gans, B.-J.; Duineveld, P. C.; Schubert, U. S. *Adv. Mater.* **2004**, *16*, 203.
(5) Beh, W. S.; Kim, I. T.; Qin, D.; Xia, Y.; Whitesides, G. M. *Adv. Mater.* **1999**, *11*, 1038.
(6) Fichet, G.; Corcoran, N.; Ho, P. K. H.; Arias, A. C.; MacKenzie, J. D.; Huck, W. T. S.; Friend, R. H. *Adv. Mater.* **2004**, *16*, 1908.
(7) Coffey, D. C.; Ginger, D. S. *J. Am. Chem. Soc.* **2005**, *127*, 4564.
(8) Gorman, C. B.; Biebuyck, H. A.; Whitesides, G. M. *Chem. Mater.* **1995**, *7*, 526.
(9) Sayre, C. N.; Collard, D. M. *J. Mater. Chem.* **1997**, *7*, 909.
(10) Sayre, C. N.; Collard, D. *Langmuir* **1997**, *13*, 714.
(11) Tao, Y.; Pandian, K.; Lee, W.-C. *Langmuir* **1998**, *14*, 6158.

(12) Rozsnyai, L. F.; Wrighton, M. S. *Langmuir* **1995**, *11*, 3913.
(13) Rozsnyai, L. F.; Wrighton, M. S. *J. Am. Chem. Soc.* **1994**, *116*, 5993.
(14) Rozsnyai, L. F.; Wrighton, M. S. *Chem. Mater.* **1996**, *8*, 309.
(15) Dalnoki-Veress, K.; Forrest, J. A.; Stevens, J. R.; Dutcher, J. R. *Physica A* **1997**, *239*, 87.
(16) Walheim, S.; Böltau, M.; Mlynek, J.; Krausch, G.; Steiner, U. *Macromolecules* **1997**, *30*, 4995.
(17) Walheim, S.; Ramstein, M.; Steiner, U. *Langmuir* **1999**, *15*, 4828.
(18) Arias, A. C.; Corcoran, N.; Banach, M.; Friend, R. H.; MacKenzie, J. D.; Huck, W. T. S. *Appl. Phys. Lett.* **2002**, *80*, 1695.
(19) Arias, A. C. J. *Macromol. Sci. Polym. Rev.* **2006**, *46*, 103.
(20) Jaczewska, J.; Budkowski, A.; Bernasik, A.; Moons, E.; Rysz, J. *Macromolecules* **2008**, *41*, 4802.
(21) Nilsson, S.; Bernasik, A.; Budkowski, A.; Moons, E. *Macromolecules* **2007**, *40*, 8291.
(22) Castro, F. A.; Graeff, C. F.O.; Heier, J.; Hany, R. *Polymer* **2007**, *48*, 2380.
(23) Castro, F. A.; Benmansour, H.; Graeff, C. F. O.; Nüesch, F.; Tutis, E.; Hany, R. *Chem. Mater.* **2006**, *18*, 5504.
(24) Han, X.; Chen, X.; Holdcroft, S. *Adv. Mater.* **2007**, *19*, 1697.
(25) Jaczewska, J.; Budkowski, A.; Bernasik, A.; Raptis, I.; Moons, E.; Goustouridis, D.; Haberko, J.; Rysz, J. *Soft Matter* **2009**, *5*, 234.
(26) Contoret, A. E. A.; Farrar, S. R.; O'Neill, M.; Nicholls, J. E.; Richards, G. J.; Kelly, S. M.; Hall, A. W. *Chem. Mater.* **2002**, *14*, 1477.
(27) Contoret, A. E. A.; Farrar, S. R.; Jackson, P. O.; Khan, S. M.; May, L.; O'Neill, M.; Nicholls, J. E.; Kelly, S. M.; Richards, G. J. *Adv. Mater.* **2000**, *12*, 971.
(28) Müller, D. C.; Braig, T.; Nothofer, H.-G.; Arnoldi, M.; Gross, M.; Scherf, U.; Nuyken, O.; Meerholz, K. *Chem. Phys. Chem.* **2000**, *1*, 207.
(29) Müller, C. D.; Falcou, A.; Reckefuss, N.; Rojahn, M.; Wiederhirn, V.; Rudati, P.; Frohne, H.; Nuyken, O.; Becker, H.; Meerholz, K. *Nature* **2003**, *421*, 829.
(30) Charas, A.; Alves, H.; Martinho, J. M. G.; Alcácer, L.; Fenwick, O.; Cacialli, F.; Morgado, J. *Synth. Met.* **2008**, *158*, 643.
(31) Charas, A.; Alcácer, L.; Pimentel, A.; Conde, J. P.; Morgado, J. *Chem. Phys. Lett.* **2008**, *455*, 189.
(32) Chua, L.-L.; Zaumseil, J.; Chang, J.-F.; Ou, E. C.-W.; Ho, P. K.-H.; Sirringhaus, H.; Friend, R. H. *Nature* **2005**, *434*, 194.
(33) Sirringhaus, H.; Wilson, R. J.; Friend, R. H.; Inbasekaran, M.; Wu, W.; Woo, E. P.; Grell, M.; Bradley, D. D. C. *Appl. Phys. Lett.* **2000**, *77*, 406.
(34) Levermore, P. A.; Jin, R.; Wang, X.; de Mello, J. C.; Bradley, D. D. C. *Adv. Funct. Mater.* **2009**, *19*, 1.
(35) Lin, H.-C.; Sung, H.-H.; Tsai, C.-M.; Li, K.-C. *Polymer* **2005**, *46*, 9810.
(36) Brédas, J. L.; Silbey, R.; Boudreaux, D. S.; Chance, R. R. *J. Am. Chem. Soc.* **1983**, *105*, 6555.
(37) Gutmann, J. S.; Müller-Buschbaum, P.; Stamm, M. *Faraday Discuss.* **1999**, *112*, 285 and references therein.
(38) Lawrence, C. J. *Phys. Fluids* **1988**, *31*, 2786.
(39) Schubert, D. W. *Polym. Bull.* **1997**, *38*, 177.
(40) Raczkowska, J.; Cyganik, P.; Budkowski, A.; Bernasik, A.; Rysz, J.; Raptis, I.; Czuba, P.; Kowalski, K. *Macromolecules* **2005**, *38*, 8486.
(41) Veress, K. D.; Forrest, J. A.; Stevens, J. R.; Dutcher, J. R. *Physica A* **1997**, *239*, 87.
(42) Geoghegan, M.; Krausch, G. *Prog. Polym. Sci.* **2003**, *28*, 261.
(43) Heriot, S. Y.; Jones, R. A. L. *Nat. Mater.* **2005**, *4*, 782.
(44) Tanaka, K.; Takahara, A.; Kajiama, T. *Macromolecules* **1996**, *29*, 3232.
(45) Geiser, A.; Bin, F.; Benmansour, H.; Castro, F.; Heier, J.; Keller, B.; Mayerhofer, K.; Karl, E.; Nüesch, F.; Hany, R. *Sol. Energy Mater. Sol. Cel.* **2008**, *92*, 464.
(46) Cheyns, D.; Vasseur, K.; Rolin, C.; Genoe, J.; Poortmans, J.; Heremans, P. *Nanotechnology* **2008**, *19*, 424016.
(47) Halls, J. J. M.; Pichler, K.; Friend, R. H.; Moratti, S. C.; Holmes, A. B. *Appl. Phys. Lett.* **1996**, *68*, 3120.
(48) Stubinger, T.; Brutting, W. *J. Appl. Phys.* **2001**, *20*, 3632.
(49) Thomas, S. W.; Joly, G. D.; Swager, T. M. *Chem. Rev.* **2007**, *107*, 1339 and references therein.
(50) Chen, L.-M.; Hong, Z.; Li, G.; Yang, Y. *Adv. Mater.* **2009**, *21*, 1 and references therein.
(51) Bernasik, A.; Włodarczyk-Miśkiewicz, J.; Łużny, W.; Kowalski, K.; Raczkowskac, J.; Rysz, J.; Budkowski, A. *Synth. Met.* **2004**, *144*, 253.
(52) Al-Ibrahim, M.; Roth, H.-K.; Zhokhavets, U.; Gobsh, G.; Sensfuss, S. *Sol. Energy Mater. Sol. Cel.* **2005**, *85*, 13.
(53) Cook, S.; Ohkita, H.; Durrant, J. R.; Kim, Y.; Benson-Smith, J. J.; Nelson, J.; Bradley, D. D. C. *Appl. Phys. Lett.* **2006**, *89*, 101128.
(54) Ma, W.; Yang, C.; Gong, X.; Lee, K.; Heeger, A. J. *Adv. Funct. Mater.* **2005**, *15*, 1617.
(55) Schilinky, P.; Waldauf, C.; Brabec, C. J. *Adv. Funct. Mater.* **2006**, *16*, 1669.
(56) Kim, Y.; Choulis, S. A.; Nelson, J.; Bradley, D. D. C.; Cook, S.; Durrant, J. R. *Appl. Phys. Lett.* **2005**, *86*, 063502.
(57) Motoi, M.; Suda, H.; Shimamura, K.; Nagahara, S.; Takei, M.; Kanoh, S. *Bull. Chem. Soc. Jpn.* **1988**, *61*, 1653.
(58) Pommerehne, J.; Vestweber, H.; Guss, W.; Mahrt, R. F.; Bässler, H.; Porsh, M.; Daub, J. *Adv. Mater.* **1995**, *7*, 551.